Supplementary:

Supplementary Table S1: A selected set of measured mass absorption coefficients (MAC) given at 550 nm and original provided wavelength. Conversion of MAC to 550 nm is performed assuming absorption Ångstrøm exponent to be 1. If no value is given for original wavelength the measurements is taken at 550 nm. Regions of measurements are given along with references for measurements.

Location	MAC [m^2 g^{-1}] (550)	MAC [m^2 g^{-1}] at reported wavelength	Reference
Large set of data	7.5 ± 1.2 and 11 m^2 g^{-1} at 550 nm for fresh and aged BC particles		Bond and Bergstrom (2006)
Urban	6.8 – 8.7		Hitzenberger et al. (2006)
Mexico City	8.7-8.9	5.5-5.6 (870)[1]	Doran et al. (2007)
Mexico	13.1	10.9 (660)	Subramanian et al. (2010)
High altitude (winter) High altitude (summer)	8.6 12.7	7.5 (630) 11 (630)	Cozic et al. (2008)
Denver	9.7	10 (532)[2]	Knox et al. (2009)
Different sites in India	7.4 – 17.3	Between 6 and 14 (at 678 nm)	Ram and Sarin (2009)
Urban (Barcelona) Traffic (Bern) Industrial (Huelva)	10.7 11.9 11.4	9.2 (637) 10.3 (637) 9.8 (637)	Reche et al. (2011)
Urban (Paris)	13.8	8.6 (880)	Laborde et al. (2013)
Shenzhen (China)	6.3	6.5 ± 0.5 (532)	Lan et al. (2013)
South Texas	7.8	8.1 (532)	Levy et al. (2013)
Arctic	5.7	around 6 (522 nm)	Yttri et al. (2014)
Rural North China	12.3	10 (678 nm)	Cui et al. (2016)
Aspvreten (SE) Birkenes (NO Finokalia (GR) Harwell (GB) Ispra (IT) Melpitz (DE) Montseny (ES) Puy de Dôme (FR) Vavihill (SE)	9.8 9.1 14.3 15.6 11.1 10.7 10.3 20.0 7.5	8.51 (637) 7.86 (637) 12.4 (637) 13.5 (637) 9.61 (637) 9.23 (637) 8.92 (637) 17.3 (637) 6.47(637)	Zanatta et al. (2016)
Fresno, Italy	7.4	7.9 ± 1.5 (532)	Presler-Jur et al. (2017)
Northwest China	13.3	8.3 (880) as an average of 7.4, 5.7, 8.1 and 12.1	Zhang et al. (2019)
Milan, Italy	9.9	10.2 (532)	Forello et al. (2019)
China	11.4	11.8 (532)	Ma et al. (2020)

[1] See correction of the publication.
[2] See value provided in Ma et al. (2020).

Supplementary text T1: Since the rapid adjustments are derived using kernel techniques it is important to assess the uncertainties in the calculations. In particular, the residuals provide information on the clouds rapid adjustments, where uncertainties are larger than for the other contributors according to Smith et al. (2018). The residual between direct model output and calculations using radiative kernels are shown in Figure S1 for model mean and individual models, and for SW, LW and Net. Since SW and LW residuals are of opposite sign, the net residuals are weakest, indicating that uncertainties are small in the rapid adjustment calculations shown in Figure 1. Residuals are stronger in magnitude in absolute and relative terms in BC STD compared to the BC VC experiment. The residuals are well within the model range for the total rapid adjustment shown in Figure 1 in the main manuscript. Maximum model range in the residual is 0.03 W m^{-2} for LW rapid adjustments. Residuals are possible to quantify for all four models for LW radiation using ERF, but for SW radiation this is available only for the three models which performed double radiation calls.

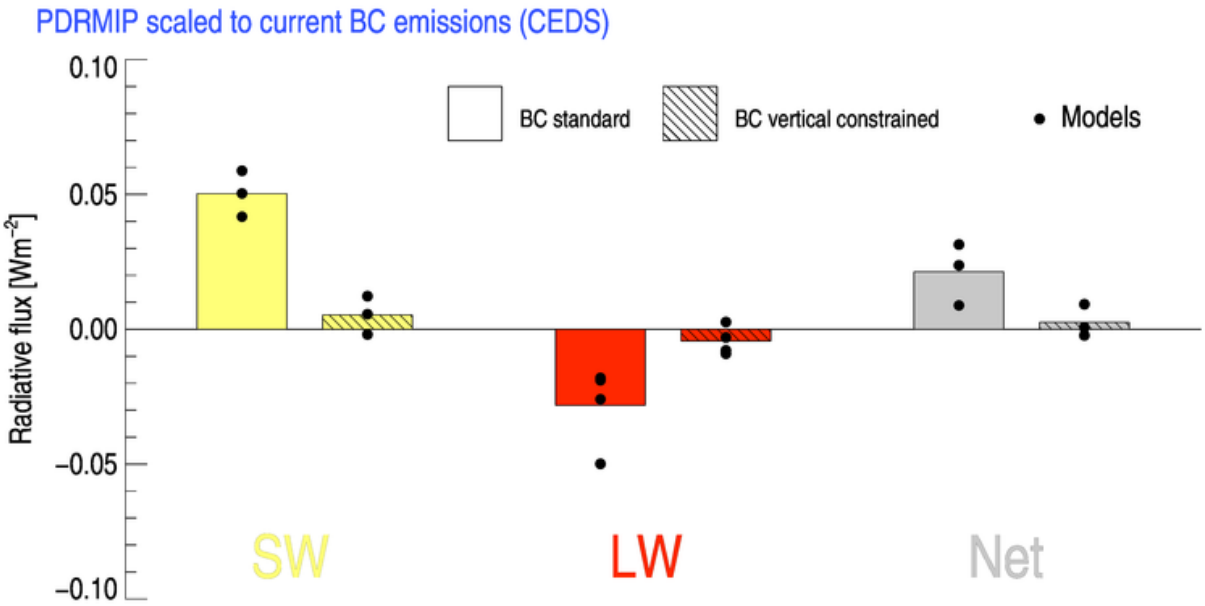

Figure S1: Global mean residuals between direct climate model results and radiative kernel calculations of rapid adjustments, divided into longwave (LW), shortwave (SW) and Net radiation from the two experiments STD (full bars) and VC (bars with lines). Individual models are shown as black dots. Three models have double radiation calls allowing derivation of residual for SW and Net. Residual between radiative kernel calculations and climate model results of rapid adjustment is derived from LW ERF since LW IRF is either zero or derived by double radiative calls.

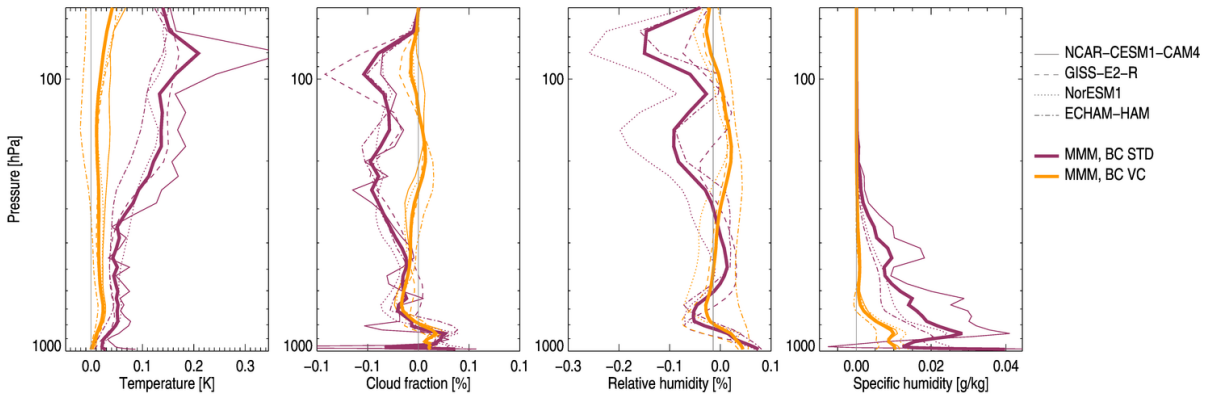

Figure S2: Like Figure 4 but showing the results from each of the four models. Atmospheric vertical profiles of changes in temperature, cloud fraction, relative humidity, and specific humidity for the two experiments BC STD and BC VC.

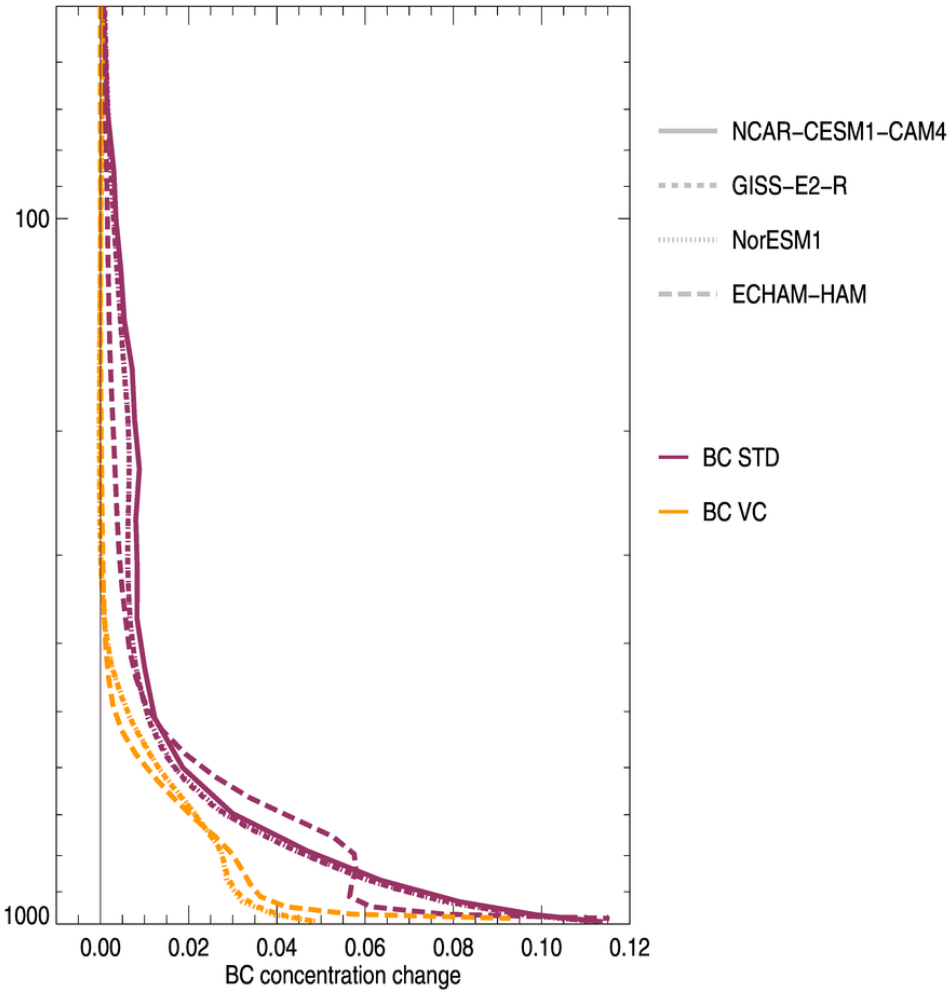

Figure S3: Atmospheric vertical profile of black carbon, for the 2 black carbon experiments. The standard vertical profile is shown in purple and vertical constrained in orange. Note the strong reduction in BC concentration at higher altitudes in the troposphere in the observationally constrained profiles. Some of the lines are overlayed in the concentration driven models.

Supplementary text T2: We have provided results from the fully coupled climate models from year 51-100 but also gave an estimate for year 20 (mean of year 18-22). The rationale for looking at year 20 is that a zero layer model provides a good fit to the historical record (e.g. Gregory and Forster (2008); Held et al. (2010)). In step change experiments the upper-layer has approximately come into equilibrium at about year 20, while the deep-ocean can still be approximated as dT ~ 0 (in a two-layer ocean model, representing the mixed-layer and deep-ocean). Hence at year 20 surface temperature change is the zero-layer model. This is further described in Section 3 of Gregory et al. (2015).

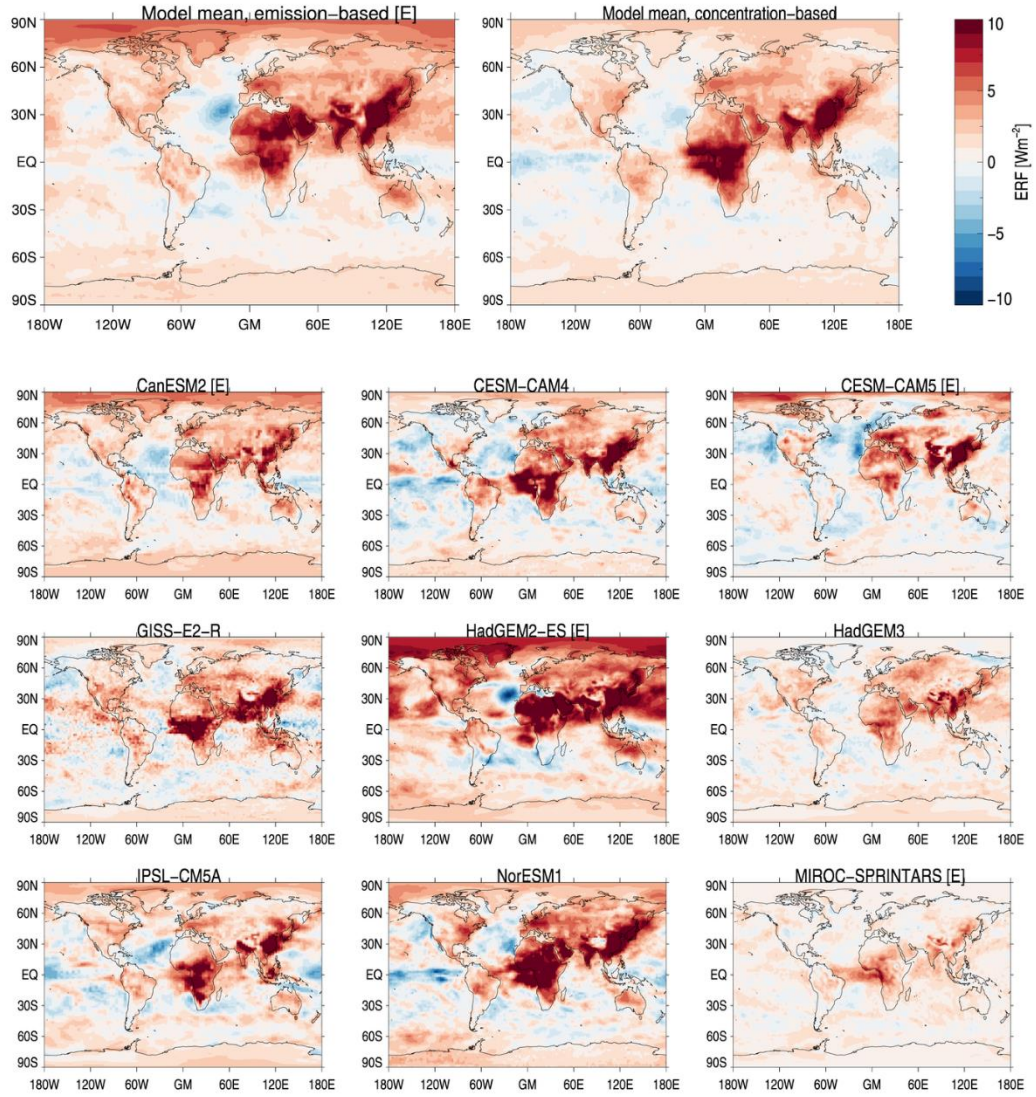

Figure S4: ERF for BC STD experiment for 9 PDRMIP models and models mean for emission driven and concentration driven models. All models are scaled to the same emissions as for the concentration driven models.

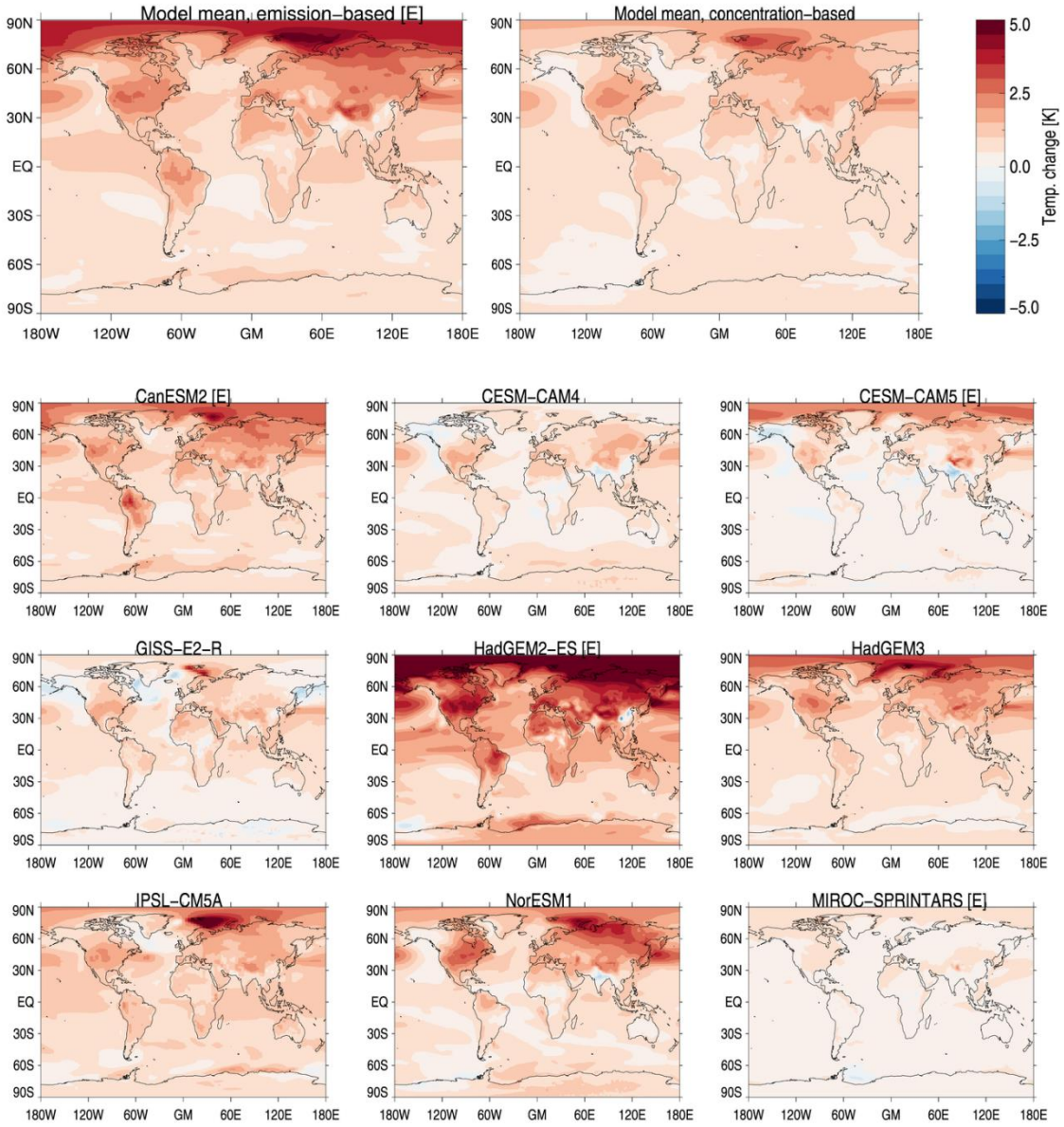

Figure S5: Surface temperature change for the BC STD experiment for 9 PDRMIP models, and model means for emission driven and concentration driven models. All models are scaled to the same emissions as for the concentration driven models.

	ERF [Wm^{-2}]	Normalized ERF [Wm-2]	Norm, ERF [Wg^{-1}]	Emission-scaled temp, change [K]
CanESM2 [E]	1.54	NA	350	0.78
CESM-CAM5 [E]	0.41	49	490	0.17
HadGEM2-ES [E]	2.91	153	490	1.51
MIROC-SPRINTARS [E]	0.65	81	330	0.11
GISS-E2-R	1.26	112	640	0.39
CESM-CAM4	0.78	59	430	0.35
HadGEM3	0.68	70	380	0.70
IPSL-CM5A	0.82	76	440	0.75
NorESM1	1.43	100	750	0.67
ECHAM-HAM	0.73	58	NA	0.24

Table S2: Global and annual mean effective radiative forcing (ERF), ERF normalized by absorption aerosol optical depth (AAOD), ERF normalized by burden, and temperature change for BCSTD experiment for 9 PDRMIP models (Stjern et al., 2017). The ECHAM-HAM results are performed for this study. Results are provided for emission driven and concentration driven models. All models are scaled to the same emissions as for the concentration driven models. Note that all results are for 10xBC and there is no scaling by mass absorption coefficient.

CEDS Emissions v2021		
	BC standard	BC vertical constrained
IRF	0.34 (0.02)	0.14 (0.02)
ERF	0.17 (0.06)	0.08 (0.05)
Rapid adjustments	-0.16 (0.06)	-0.06 (0.03)
Surface temperature change	0.07 (0.03)	0.03 (0.02)
CEDS Emissions v2016		
IRF	0.47 (0.03)	0.20 (0.03)
ERF	0.24 (0.08)	0.11 (0.06)
Rapid adjustments	-0.22 (0.08)	-0.08 (0.05)
Surface temperature change	0.10 (0.04)	0.04 (0.03)

Table S3: Multi-model global and annual mean instantaneous radiative forcing (IRF), effective radiative forcing (ERF), rapid adjustment, surface temperature for the BC standard and BC vertical constrained experiments. Numbers in parentheses are one standard deviation from the four models in this study. Results are shown for CEDS emission versions from 2021 and 2016 (applied in CMIP6).

Bond, T. C. and Bergstrom, R. W.: Light absorption by carbonaceous particles: An investigative review, Aerosol Science And Technology, 40(1), 27-67, 2006.

Cozic, J., Verheggen, B., Weingartner, E., Crosier, J., Bower, K. N., Flynn, M., Coe, H., Henning, S., Steinbacher, M., Henne, S., Collaud Coen, M., Petzold, A. and Baltensperger, U.: Chemical composition of free tropospheric aerosol for PM1 and coarse mode at the high alpine site Jungfraujoch, Atmos. Chem. Phys., 8(2), 407-423, 2008.

Cui, X., Wang, X., Yang, L., Chen, B., Chen, J., Andersson, A. and Gustafsson, Ö.: Radiative absorption enhancement from coatings on black carbon aerosols, Science of The Total Environment, 551–552, 51-56, 2016.

Doran, J. C., Barnard, J. C., Arnott, W. P., Cary, R., Coulter, R., Fast, J. D., Kassianov, E. I., Kleinman, L., Laulainen, N. S., Martin, T., Paredes-Miranda, G., Pekour, M. S., Shaw, W. J., Smith, D. F., Springston, S. R. and Yu, X. Y.: The T1-T2 study: evolution of aerosol properties downwind of Mexico City, Atmos. Chem. Phys., 7(6), 1585-1598, 2007.

Forello, A. C., Bernardoni, V., Calzolai, G., Lucarelli, F., Massabò, D., Nava, S., Pileci, R. E., Prati, P., Valentini, S., Valli, G. and Vecchi, R.: Exploiting multi-wavelength aerosol absorption coefficients in a multi-time resolution source apportionment study to retrieve source-dependent absorption parameters, Atmos. Chem. Phys., 19(17), 11235-11252, 2019.

Gregory, J. M., Andrews, T. and Good, P.: The inconstancy of the transient climate response parameter under increasing CO₂, Philosophical Transactions of the Royal Society A: Mathematical, Physical and Engineering Sciences, 373(2054), 20140417, 2015.

Gregory, J. M. and Forster, P. M.: Transient climate response estimated from radiative forcing and observed temperature change, Journal of Geophysical Research-Atmospheres, 113(D23), D23105, 2008.

Held, I. M., Winton, M., Takahashi, K., Delworth, T., Zeng, F. and Vallis, G. K.: Probing the Fast and Slow Components of Global Warming by Returning Abruptly to Preindustrial Forcing, Journal of Climate, 23(9), 2418-2427, 2010.

Hitzenberger, R., Petzold, A., Bauer, H., Ctyroky, P., Pouresmaeil, P., Laskus, L. and Puxbaum, H.: Intercomparison of Thermal and Optical Measurement Methods for Elemental Carbon and Black Carbon at an Urban Location, Environmental Science & Technology, 40(20), 6377-6383, 2006.

Knox, A., Evans, G. J., Brook, J. R., Yao, X., Jeong, C. H., Godri, K. J., Sabaliauskas, K. and Slowik, J. G.: Mass Absorption Cross-Section of Ambient Black Carbon Aerosol in Relation to Chemical Age, Aerosol Science and Technology, 43(6), 522-532, 2009.

Laborde, M., Crippa, M., Tritscher, T., Jurányi, Z., Decarlo, P. F., Temime-Roussel, B., Marchand, N., Eckhardt, S., Stohl, A., Baltensperger, U., Prévôt, A. S. H., Weingartner, E. and Gysel, M.: Black carbon physical properties and mixing state in the European megacity Paris, Atmos. Chem. Phys., 13(11), 5831-5856, 2013.

Lan, Z.-J., Huang, X.-F., Yu, K.-Y., Sun, T.-L., Zeng, L.-W. and Hu, M.: Light absorption of black carbon aerosol and its enhancement by mixing state in an urban atmosphere in South China, Atmospheric Environment, 69, 118-123, 2013.

Levy, M. E., Zhang, R., Khalizov, A. F., Zheng, J., Collins, D. R., Glen, C. R., Wang, Y., Yu, X.-Y., Luke, W., Jayne, J. T. and Olaguer, E.: Measurements of submicron aerosols in Houston, Texas during the 2009 SHARP field campaign, Journal of Geophysical Research: Atmospheres, 118(18), 10,518-10,534, 2013.

Ma, Y., Huang, C., Jabbour, H., Zheng, Z., Wang, Y., Jiang, Y., Zhu, W., Ge, X., Collier, S. and Zheng, J.: Mixing state and light absorption enhancement of black carbon aerosols in summertime Nanjing, China, Atmospheric Environment, 222, 117141, 2020.

Presler-Jur, P., Doraiswamy, P., Hammond, O. and Rice, J.: An evaluation of mass absorption cross-section for optical carbon analysis on Teflon filter media, Journal of the Air & Waste Management Association, 67(11), 1213-1228, 2017.

Ram, K. and Sarin, M. M.: Absorption Coefficient and Site-Specific Mass Absorption Efficiency of Elemental Carbon in Aerosols over Urban, Rural, and High-Altitude Sites in India, Environmental Science & Technology, 43(21), 8233-8239, 2009.

Reche, C., Querol, X., Alastuey, A., Viana, M., Pey, J., Moreno, T., Rodríguez, S., González, Y., Fernández-Camacho, R., de la Rosa, J., Dall'Osto, M., Prévôt, A. S. H., Hueglin, C., Harrison, R. M. and Quincey, P.: New considerations for PM, Black Carbon and particle number concentration for air quality monitoring across different European cities, Atmos. Chem. Phys., 11(13), 6207-6227, 2011.

Smith, C. J., Kramer, R. J., Myhre, G., Forster, P. M., Soden, B. J., Andrews, T., Boucher, O., Faluvegi, G., Fläschner, D., Hodnebrog, Ø., Kasoar, M., Kharin, V., Kirkevåg, A., Lamarque, J.-F., Mülmenstädt, J., Olivié, D., Richardson, T., Samset, B. H., Shindell, D., Stier, P., Takemura, T., Voulgarakis, A. and Watson-Parris, D.: Understanding Rapid Adjustments to Diverse Forcing Agents, Geophysical Research Letters, 45(21), 12,023-12,031, 2018.

Stjern, C. W., Samset, B. H., Myhre, G., Forster, P. M., Hodnebrog, Ø., Andrews, T., Boucher, O., Faluvegi, G., Iversen, T., Kasoar, M., Kharin, V., Kirkevåg, A., Lamarque, J.-F., Olivié, D., Richardson, T., Shawki, D., Shindell, D., Smith, C. J., Takemura, T. and Voulgarakis, A.: Rapid Adjustments Cause Weak Surface Temperature Response to Increased Black Carbon Concentrations, Journal of Geophysical Research: Atmospheres, 122(21), 11462-11481, 2017.

Subramanian, R., Kok, G. L., Baumgardner, D., Clarke, A., Shinozuka, Y., Campos, T. L., Heizer, C. G., Stephens, B. B., de Foy, B., Voss, P. B. and Zaveri, R. A.: Black carbon over Mexico: the effect of atmospheric transport on mixing state, mass absorption cross-section, and BC/CO ratios, Atmos. Chem. Phys., 10(1), 219-237, 2010.

Yttri, K. E., Lund Myhre, C., Eckhardt, S., Fiebig, M., Dye, C., Hirdman, D., Ström, J., Klimont, Z. and Stohl, A.: Quantifying black carbon from biomass burning by means of levoglucosan – a one-year time series at the Arctic observatory Zeppelin, Atmos. Chem. Phys., 14(12), 6427-6442, 2014.

Zanatta, M., Gysel, M., Bukowiecki, N., Müller, T., Weingartner, E., Areskoug, H., Fiebig, M., Yttri, K. E., Mihalopoulos, N., Kouvarakis, G., Beddows, D., Harrison, R. M., Cavalli, F., Putaud, J. P., Spindler, G., Wiedensohler, A., Alastuey, A., Pandolfi, M., Sellegri, K., Swietlicki, E., Jaffrezo, J. L., Baltensperger, U. and Laj, P.: A European aerosol phenomenology-5: Climatology of black carbon optical properties at 9 regional background sites across Europe, Atmospheric Environment, 145(Supplement C), 346-364, 2016.

Zhang, Q., Shen, Z., Lei, Y., Zhang, T., Zeng, Y., Ning, Z., Sun, J., Westerdahl, D., Xu, H., Wang, Q., Cao, J. and Zhang, R.: Optical properties and source identification of black carbon and brown carbon: comparison of winter and summer haze episodes in Xi'an, Northwest China, Environmental Science: Processes & Impacts, 21(12), 2058-2069, 2019.